REPORT
doi:10.26443/seismica.v3i2.1405

Earthquake source inversion by integrated fiber-optic sensing

Nils Mueller [1], **Sebastian Noe** [1], **Dominik Husmann** [2], **Jacques Morel** [2], **Andreas Fichtner** [*1]

[1]Department of Earth Sciences, ETH Zurich, Zurich, Switzerland, [2]Swiss Federal Institute of Metrology, METAS, Bern, Switzerland

Author contributions: *Conceptualization*: Andreas Fichtner, Dominik Husmann, Jacques Morel. *Methodology*: Andreas Fichtner. *Software*: Sebastian Noe, Nils Mueller. *Formal Analysis*: Nils Mueller, Sebastian Noe. *Investigation*: Nils Mueller, Sebastian Noe. *Resources*: Andreas Fichtner, Dominik Husmann, Jacques Morel. *Writing - Original draft*: Andreas Fichtner, Nils Mueller, Sebastian Noe, Dominik Husmann, Jacques Morel.

Abstract We present an earthquake source inversion using a single time series produced by integrated fiber-optic sensing in a phase noise cancellation (PNC) system used for frequency metrology. Operating on a 123 km long fiber between Bern and Basel (Switzerland), the PNC system recorded the M_w3.9 Mulhouse earthquake that occurred on 10 September 2022 around 10 km north-west of the northern fiber end. A generalised least-squares inversion in the 4 - 13 s period band constrains the components of a double-couple moment tensor with an uncertainty that corresponds to ∼0.2 moment magnitude units, nearly independent of prior information. Uncertainties for hypocenter location and original time are more variable, ranging between 4 - 20 km and 0.1 - 1 s, respectively, depending on whether injected prior information is realistic or almost absent. This work is a proof of concept that quantifies the resolvability of earthquake source properties under specific conditions using a single-channel stand-alone integrated (non-distributed) fiber-optic measurement. It thereby constitutes a step towards the integration of long-range phase-transmission fiber-optic sensors into existing seismic networks in order to fill significant seismic data gaps, especially in the oceans.

Production Editor:
Kiran Kumar Thingbaijam
Ryo Okuwaki
Handling Editor:
Kiran Kumar Thingbaijam
Copy & Layout Editor:
Théa Ragon

Signed reviewer(s):
Martijn van den Ende

Received:
June 28, 2024
Accepted:
July 15, 2024
Published:
July 22, 2024

1 Introduction

Fiber-optic deformation sensing promises to close important seismic data gaps. The most widespread technology, Distributed Acoustic Sensing (DAS), offers a channel spacing in the meter range and a frequency bandwidth from milli- to kilohertz (e.g., Hartog, 2017; Lindsey et al., 2020; Paitz et al., 2021), which is often difficult to achieve with conventional seismometers. Using specially deployed fiber-optic cables or leveraging existing telecommunication infrastructure, DAS has opened up new opportunities in urban seismology (e.g., Dou et al., 2017; Spica et al., 2020b; Fang et al., 2020; Bowden et al., 2024), volcanology (e.g., Jousset et al., 2018; Klaasen et al., 2021; Jousset et al., 2022; Klaasen et al., 2023), glaciology (e.g., Walter et al., 2020; Fichtner et al., 2023b,a; Hudson et al., 2021; Brisbourne et al., 2021) and many others. While DAS is being used in underwater applications (e.g., Sladen et al., 2019; Spica et al., 2020a; Cheng et al., 2021; Lior et al., 2021; Igel et al., 2024), its range limitation to typically several tens of kilometers, still prevents the closure of the most prominent data gap: the oceans.

Alternatives to DAS that potentially offer a longer range have been developed in recent years. They mostly rest on the measurement of polarization (e.g., Mecozzi et al., 2021; Zhan et al., 2021) or phase (e.g., Marra et al., 2018; Bogris et al., 2022; Noe et al., 2023; Donadello et al., 2024) in forward transmitted optical signals, thereby providing a single time series that integrates axial strain along the fiber. The integrated, i.e., not spatially distributed, nature of the data complicates the most fundamental seismological task: earthquake source characterization. Marra et al. (2018) proposed several earthquake location approaches using either bidirectional integrated fiber-optic sensors or multiple cables. However, none of these ideas has been implemented so far.

Here we present an earthquake source inversion for location, moment tensor and origin time using an integrated fiber-optic sensing system based on active phase noise cancellation (PNC) in metrological frequency dissemination (Husmann et al., 2021; Noe et al., 2023). Deployed on a 123 km long fiber link between the cities of Bern and Basel in Switzerland, the sensing system couses real-time corrections of deformation-induced frequency shifts, which are a side product of the metrological service, and hence allows simultaneous operation without the need of additional devices.

2 Experimental setup

We briefly summarize the measurement system, referring to previous publications for details (Husmann et al., 2021; Noe et al., 2023). At its origin, the fiber network used here was established for metrological frequency dissemination. It enables the dissemination of ultrastable and accurate optical reference frequencies

*Corresponding author: andreas.fichtner@erdw.ethz.ch

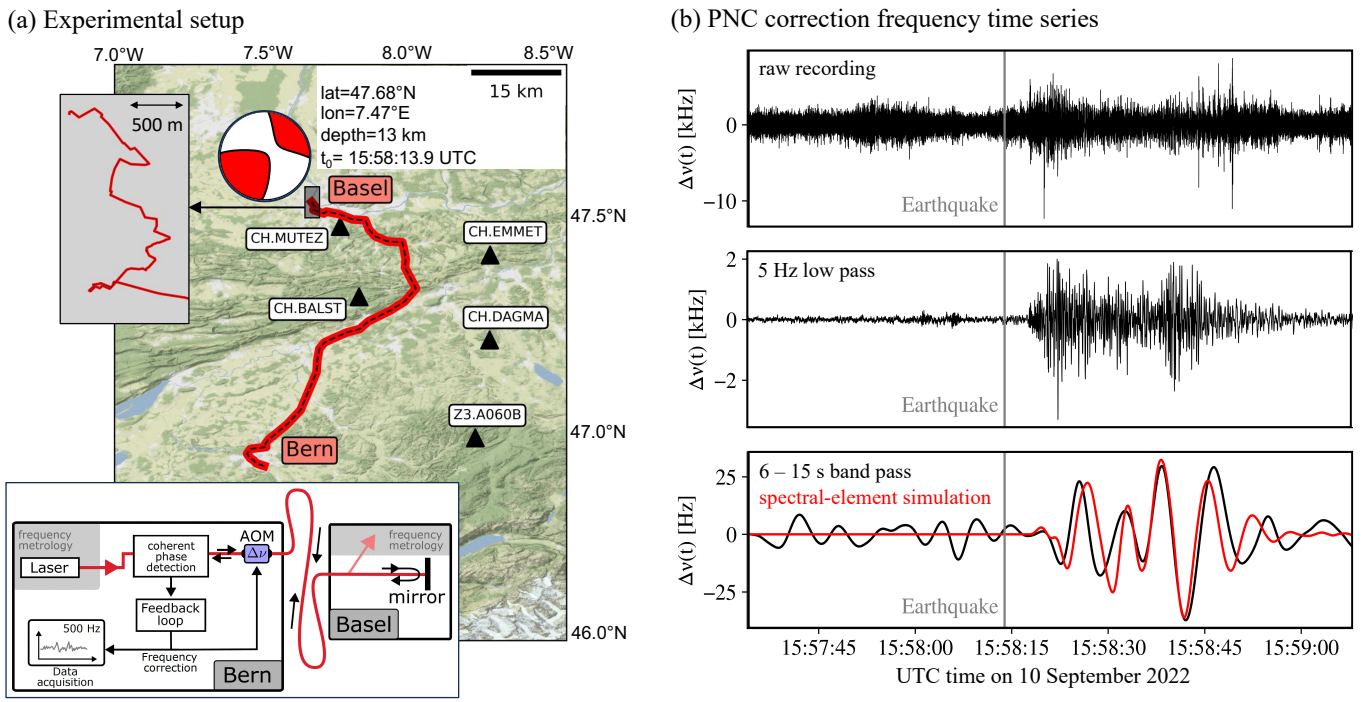

Figure 1 Summary of the PNC sensing experiment in the context of the M3.9 Mulhouse earthquake. (a) The PNC system operates on a 123 km long fiber network segment (red curve). The upper inset focuses on the complex cable geometry in the city center of Basel, which was accurately implemented in the spectral-element solver Salvus (Afanasiev et al., 2019). The moment tensor estimate shown on the map was provided by GEOFON (Hanka and Kind, 1994), and the location by the Swiss Seismological Service (SED, 2024). Broadband stations (black triangles) were used to adjust the 1-D Earth model of the Alpine region by (Diehl et al., 2009) to our area of interest (Noe et al., 2023). The lower inset shows the PNC system. The laser is part of the frequency metrology infrastructure at METAS, and stabilized on an ultralow expansion cavity. The PNC consists of coherent phase detection based on a Michelson-type interferometer, a feedback loop and a frequency correction $\Delta\nu(t)$ applied via an acousto-optic modulator (AOM). In Basel, part of the light is coupled out for local use in frequency metrology, while the rest is reflected back by a mirror. (b) Raw and filtered times series of the correction frequency $\Delta\nu(t)$. The red time series has been computed with Salvus, using the earthquake source estimate from panel (a).

traceable to the SI definition of the second, from the Swiss Federal Institute of Metrology (METAS) to user laboratories performing precision spectroscopy measurements. Temperature variations and deformation of the fiber perturb the received frequency, thereby producing phase noise that motivates the recent development of PNC systems (e.g., Calonico et al., 2014; BACON Collaboration et al., 2021; Cantin et al., 2021; Cizek et al., 2022; Schioppo et al., 2022). Our PNC implementation, illustrated in Fig. 1a, rests on a coherent optical phase measurement and feedback loop acting on the optical frequency. A continuous-wave laser signal is sent from a local to a remote station. At the remote station, part of the signal is coupled out for metrological applications, and the remainder is reflected back to the local station for comparison with the emitted signal. The frequency shift, $\Delta\nu$, between in- and out-going signals is proportional to the integral of axial strain rate, $\dot{\varepsilon}$, along the fiber of length L,

$$\Delta\nu(t) = \frac{4\pi\nu}{c}\int_{\ell=0}^{L}\dot{\varepsilon}(\ell,t)\,d\ell\,, \qquad (1)$$

where $\nu = 190.7$ THz and $c = 204.2\cdot10^6$ m/s are the emitted frequency and the speed of light in the fiber, respectively.

Our PNC system operates on a 2×123 km loop, connecting METAS to the University of Bern (Fig. 1a). On 10 September 2022, the system recorded the M_w3.9 Mulhouse earthquake, located ∼10 km north-west of the northern end of the fiber. As illustrated in Fig. 1b, raw correction frequencies $\Delta\nu$, measured with 500 samples per second, are on the order of several kHz. In the 6 - 15 s period band, where the signal-to-noise ratio (SNR) is higher and observations can be compared to simulations (Noe et al., 2023), $\Delta\nu$ is at the level of few tens of Hz.

3 Earthquake source inversion setup

The recording of the Mulhouse event allows us to quantify the capability of an integrated fiber-optic sensing system to constrain earthquake source parameters. For this, we compute numerical Green's functions and their partial derivatives $\mathbf{G}$ with respect to source parameters using the spectral-element solver Salvus (Afanasiev et al., 2019). As Earth model, we employ the 1-D model of the Alpine region (Diehl et al., 2009), slightly modified to better explain waveforms at nearby broadband stations (black triangles in Fig. 1a) in the 3 - 30 s period band (Noe et al., 2023). Furthermore, we implement topographic variations and the complex fiber geometry.

Since the PNC time series has a useful SNR at periods

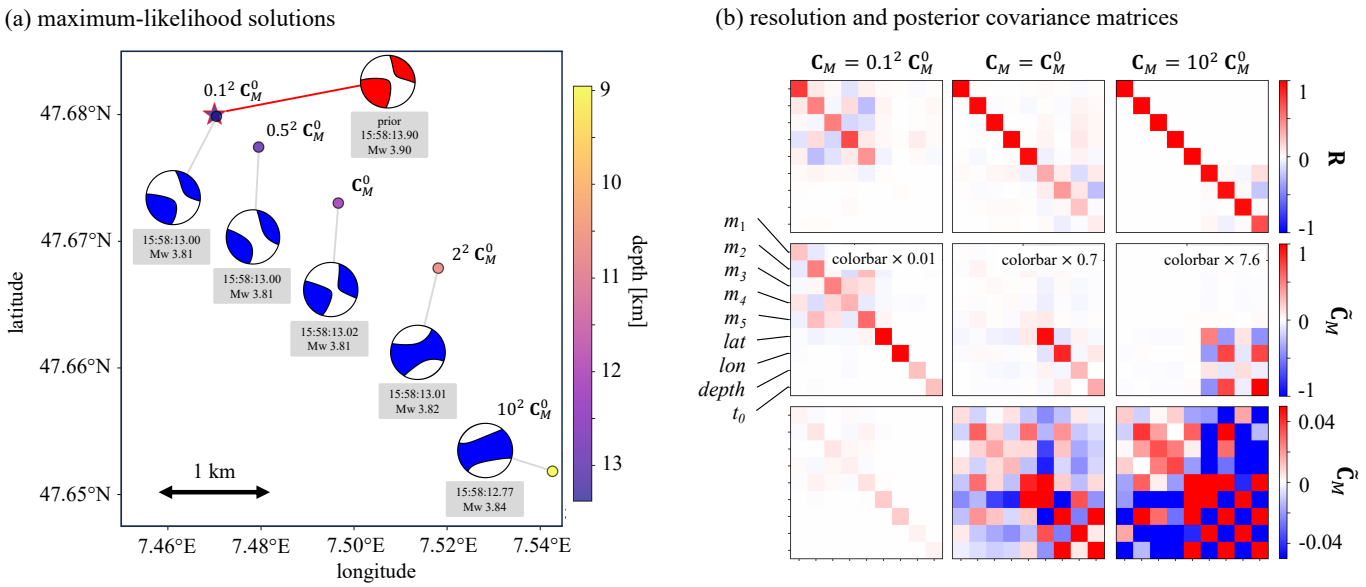

Figure 2 Source inversion results for different choices of the prior model covariance $\mathbf{C}_M = \gamma^2\,\mathbf{C}_M^0$, with γ ranging from 0.1 (strong prior) to 10 (weak prior). (a) Maximum-likelihood source parameters. The prior model is shown as red beach ball (location from SED (2024), moment tensor from GEOFON (Hanka and Kind, 1994)). (b) Resolution matrix $\mathbf{R}$ (top row) and posterior model covariance matrix $\tilde{\mathbf{C}}_M$ (middle and bottom rows, corresponding to different color scale options). To facilitate the interpretation, the matrix elements $(\tilde{\mathbf{C}}_M)_{ij}$ in the plot are divided by $\sigma_i^0\sigma_j^0$, where $\sigma_i^0 = \sqrt{(\mathbf{C}_M^0)_{ii}}$ are the prior standard deviations of the baseline covariance $\mathbf{C}_M^0$.

between 4 - 13 s, we construct the observed data vector $\mathbf{d}^{\text{obs}}$ by concatenating bandpass filtered versions of the recording between 4 - 6 s, 5 - 7 s, ..., and 11 - 13 s. The entries of the data covariance matrix $\mathbf{C}_D$ are estimated from the pre-event noise statistics in these period bands. Using $\mathbf{d}^{\text{obs}}$, we aim to constrain the origin time, event location and the double-couple moment tensor $\mathbf{M}$, parametrized in terms of the five elementary moment tensors (Kikuchi and Kanamori, 1991)

$$\mathbf{M}_1 = \begin{pmatrix} 0 & 1 & 0 \\ 1 & 0 & 0 \\ 0 & 0 & 0 \end{pmatrix}, \mathbf{M}_2 = \begin{pmatrix} 1 & 0 & 0 \\ 0 & -1 & 0 \\ 0 & 0 & 0 \end{pmatrix},$$
$$\mathbf{M}_3 = \begin{pmatrix} 0 & 0 & 0 \\ 0 & 0 & 1 \\ 0 & 1 & 0 \end{pmatrix}, \mathbf{M}_4 = \begin{pmatrix} 0 & 0 & 1 \\ 0 & 0 & 0 \\ 1 & 0 & 0 \end{pmatrix}, \quad (2)$$
$$\mathbf{M}_5 = \begin{pmatrix} -1 & 0 & 0 \\ 0 & 0 & 0 \\ 0 & 0 & 1 \end{pmatrix},$$

such that $\mathbf{M} = \sum_{i=1}^{5} m_i \mathbf{M}_i$, with the unknown coefficients m_i. We omit the sixth elementary moment tensor $\mathbf{M}_6 = \mathbf{I}$, which describes a purely isotropic source mechanism that we exclude *a priori*. In terms of m_i, the moment tensor in Fig. 1a given by GEOFON (Hanka and Kind, 1994) is $m_1 = 7.77 \cdot 10^{14}$ Nm, $m_2 = -8.09 \cdot 10^{13}$, Nm $m_3 = -1.73 \cdot 10^{14}$ Nm, $m_4 = -1.83 \cdot 10^{14}$ Nm, $m_5 = 2.52 \cdot 10^{13}$ Nm. The prior model covariance matrix $\mathbf{C}_M$ encapsulates prior knowledge included in the inverse problem solution. To assess how different choices of $\mathbf{C}_M$ affect the solution, we first define a diagonal baseline covariance $\mathbf{C}_M^0$ with entries $(\mathbf{C}_M^0)_{11,\ldots,55} = (1{\cdot}10^{16}\ \text{Nm})^2$ (moment tensor coefficients), $(\mathbf{C}_M^0)_{66,77} = (10\ \text{km})^2$ (northing, easting), $(\mathbf{C}_M^0)_{88} = (5\ \text{km})^2$ (depth) and $(\mathbf{C}_M^0)_{99} = (0.5\ \text{s})^2$ (origin time). The prior model covariance used in various inversions is then defined as $\mathbf{C}_M = \gamma^2\,\mathbf{C}_M^0$, with the scalar γ ranging from 0.1 to 10. Taking the source parameters summarized in Fig. 1a as a reference, $\gamma = 1$ is what we already consider a slightly weak prior, relative to uncertainties reported in catalogs (Hanka and Kind, 1994; SED, 2024). Hence, inversions with $\gamma = 1$ can be interpreted as updates of previously available information, whereas $\gamma = 10$ corresponds to inversions where prior information from catalogs plays a minor role. To estimate the unknown source parameters, we perform a generalized least-squares inversion (Tarantola and Valette, 1982), which allows us to compute the resolution matrix $\mathbf{R}$ and the posterior covariance matrix $\tilde{\mathbf{C}}_M$, in addition to the maximum-likelihood model.

4 Inversion results

Fig. 2 summarizes inversion results for different choices of $\mathbf{C}_M = \gamma^2\,\mathbf{C}_M^0$ with γ ranging from 0.1 to 10. Despite varying prior standard deviations by a factor of 100, maximum-likelihood moment tensor components only differ within few tens of percent, hypocenter location by few kilometers, and origin time by less than 1 s. In the case of realistic prior knowledge, i.e., $\gamma = 1$, the resolution matrix $\mathbf{R}$ indicates that the $m_{i=1,\ldots,5}$ are nearly independently resolved, whereas the space-time constraints are blurred. This is also reflected in the posterior covariance $\tilde{\mathbf{C}}_M$, which indicates larger inter-parameter trade-offs for location and time than for the moment tensor components. Posterior standard deviations are around (10^{15}) Nm for the moment tensor components (∼0.2 moment magnitude units), ∼4 km for latitude and longitude, ∼1 km for depth, and ∼0.1 s for ori-

gin time.

The case of excessively weak prior knowledge, γ=10, permits a location search radius on the order of 100 km, time shifts of several seconds, and magnitude variations of around 1.5 moment magnitude units. Despite these weak prior constraints, $\mathbf{R}$ is close to the unit matrix, meaning that an error-free synthetic source inversion would be capable of reproducing any input model almost exactly. Posterior covariances for the moment tensor components and for depth are similar to those estimated in the γ=1 scenario, suggesting that they are indeed constrained by the data and not by the prior. However, posterior standard deviations for the other parameters increase to $\sim$20 km for latitude and longitude, and $\sim$1 s for origin time.

Setting γ=0.1 produces an unrealistic case of excessively strong prior knowledge that primarily serves to test the proper functioning of the inversion procedure. As expected, posterior covariances decrease substantially because (apparent) certainty is enforced by the prior. The resolution matrix $\mathbf{R}$ differs strongly from the unit matrix because any estimated model is close to the prior model, even when the data would favour a different solution.

5 Discussion

PNC provides a single time series of strain rate integrated along the fiber, which seemingly precludes source location by triangulation. The ability of PNC to still constrain earthquake source parameters is rooted in the measurement sensitivity of all phase transmission fiber-optic deformation sensors (e.g., Marra et al., 2018; Bogris et al., 2022; Noe et al., 2023; Donadello et al., 2024), which is proportional to the local fiber curvature (Fichtner et al., 2022; Bowden et al., 2022). Fiber segments with strong curvature make a larger contribution to the measurement than segments that are rather straight. As the wavefield propagates along the fiber, the ensemble of high-curvature segments therefore effectively acts as a spatially distributed measurement array. In this sense, the $\Delta\nu$ time series may be interpreted as a superposition of time series, with each individual one contributed when the wave reaches a high-curvature segment of the fiber. Hence, the geometric complexity of our fiber-loop mimics a distributed array.

In addition to this geometric aspect, the resolvability of source parameters results from the good SNR of around 10 or above in a period range where we can numerically simulate the data, and the proximity of the event to the fiber. As for any other array, resolution must decay as the distance to the event exceeds the aperture. A detailed study of how the cable geometry influences the effective array response function and the position-dependent resolvability of various source parameters, is a topic of ongoing research.

Generalized least-squares inversions require prior knowledge, which we extracted from existing earthquake catalogs. In future applications, the provenance of prior knowledge will depend on the use case. When PNC or other integrated fiber-optic sensors are operated as stand-alone systems, prior information may most easily and rapidly be obtained from a coarse grid search with a simplified Earth model. In scenarios where integrated fiber-optic sensors are part of a heterogeneous sensing system, prior information may alternatively be extracted from the standard inversion of seismometer data or beamforming. Fiber-optic sensors would then contribute additional data that further improve resolution.

This work constitutes a proof of concept that establishes the extent to which earthquake source properties can be resolved under specific conditions using only a phase transmission fiber-optic sensing system. One of the next steps would be a systematic study on source parameter resolvability as a function of fiber geometry and event location. Future applications should not only use significantly longer fiber-loops but also integrate information from additional fiber-optic systems, as well as conventional seismic sensors in order to reach optimal results and eventually contribute to the closure of significant seismic data gaps.

Acknowledgements

We gratefully acknowledge Matijn van den Ende and an anonymous reviewer for the fast and constructive feedback on the original version of this paper. We thank the group of Prof. Stefan Willitsch and his group for continued support with the PNC installation in Basel. We acknowledge SWITCH for providing the fiber network infrastructure and its geo data, and Fabian Mauchle for technical support with the network, as well as many fruitful discussions with Daniel Bowden, Sixtine Dromigny, Pascal Edme, Sara Klaasen, Patrick Paitz, Krystyna Smolinski, Jerome Faist, Ernst Heiri, Fabian Mauchle, Ziv Meir, Frédéric Merkt, Giacomo Scalari and Stefan Willitsch. Funding was provided by the European Union's Horizon 2020 research and innovation program under the Marie Sklodowska-Curie grant agreement No. 955515 (SPIN ITN), and by the Swiss National Science Foundation (SNSF) Sinergia grant CRSII5_183579.

Data and code availability

The raw correction frequency recordings of the Mulhouse earthquake are openly and freely available in the supplementary material of Noe et al. (2023).

Competing interests

There are no competing interests.

References

Afanasiev, M. V., Boehm, C., van Driel, M., Krischer, L., Rietmann, M., May, D. A., Knepley, M. G., and Fichtner, A. Modular and flexible spectral-element waveform modelling in two and three dimensions. *Geophys. J. Int.*, 216, 2019. doi: 10.1093/gji/ggy469.

BACON Collaboration, Beloy, K., Bodine, M. I., Bothwell, T., Brewer, S. M., Bromley, S. L., Chen, J.-S., Deschênes, J.-D., Diddams, S. A., Fasano, R. J., Fortier, T. M., Hassan, Y. S., Hume, D. B., Kedar, D., Kennedy, C. J., Khader, I., Koepke, A., Leibrandt, D. R.,

Leopardi, H., Ludlow, A. D., McGrew, W. F., Milner, W. R., Newbury, N. R., Nicolodi, D., Oelker, E., Parker, T. E., Robinson, J. M., Romisch, S., Schäffer, S. A., Sherman, J. A., Sinclair, L. C., Sonderhouse, L., Swann, W. C., Yao, J., Ye, J., and Zhang, X. Frequency ratio measurements at 18-digit accuracy using an optical clock network. *Nature*, 591(7851):564–569, 2021. doi: 10.1038/s41586-021-03253-4.

Bogris, A., Nikas, T., Simos, C., Simos, I., Lentas, K., Melis, N. S., Fichtner, A., Bowden, D., Smolinski, K., Mesaritakis, C., and Chochliouros, I. Sensitive seismic sensors based on microwave frequency fiber interferometry in commercially deployed cables. *Sci. Rep.*, 12, 2022. doi: 10.1038/s41598-022-18130-x.

Bowden, D. C., Fichtner, A., Nikas, T., Bogris, A., Simos, C., Smolinski, K., Lentas, K., Simos, I., and Melis, N. S. Linking distributed and integrated fiber-optic sensing. *Geophys. Res. Lett.*, 49, 2022. doi: 10.1029/2022GL098727.

Bowden, D. C., Bozdag, E., Shaiksulaiman, A., Fichtner, A., and Konca, O. Telecom fibers are sensing earthquake hazards in Istanbul. *EOS*, 105, 2024. doi: 10.1029/2024EO240219.

Brisbourne, A. M., Kendall, M., Kufner, S.-K., Hudson, T. S., and Smith, A. M. Downhole distributed acoustic profiling at the Skytrain Ice Rise, West Antarctica. *The Cryosphere*, 15, 2021. doi: 10.5194/tc-15-3443-2021.

Calonico, D., Bertacco, E. K., Calosso, C. E., Clivati, C., Costanzo, G. A., Frittelli, M., Godone, A., Mura, A., Poli, N., Sutyrin, D. V., Tino, G., Zucco, M. E., and Levi, F. High-accuracy coherent optical frequency transfer over a doubled 642-km fiber link. *Appl. Phys. B*, 117:979–986, 2014. doi: 10.1007/s00340-014-5917-8.

Cantin, E., Tønnes, M., Targat, R. L., Amy-Klein, A., Lopez, O., and Pottie, P.-E. An accurate and robust metrological network for coherent optical frequency dissemination. *New Journal of Physics*, 23(5), 2021. doi: 10.1088/1367-2630/abe79e.

Cheng, F., Chi, B., Lindsey, N., Dawe, T. C., and Ajo-Franklin, J. Utilizing distributed acoustic sensing and ocean bottom fiber optic cables for submarine structural characterization. *Sci. Rep.*, 2021. doi: doi:10.1038/s41598-021-84845-y.

Cizek, M., Pravdova, L., Pham, T. M., Lesundak, A., Hrabina, J., Lazar, J., Pronebner, T., Pronebner, T., Aeikens, E., Premper, J., Havlis, O., Velc, R., Smotlacha, V., Altmannova, L., Schumm, T., Vojtech, J., Niessner, A., and Cip, O. Coherent fibre link for synchronization of delocalized atomic clocks. *Optics Express*, 30: 5450–5464, 2022. doi: 10.1364/OE.447498.

Diehl, T., Kissling, E., Husen, S., and Aldersons, F. Consistent phase picking for regional tomography models: application to the greater Alpine region. *Geophys. J. Int.*, 176:542–554, 2009. doi: 10.1111/j.1365-246X.2008.03985.x.

Donadello, S., Clivati, C., Govoni, A., Margheriti, L., Vassallo, M., Brenda, D., Hovsepyan, M., Bertacco, E. K., Concas, R., Levi, F., Mura, A., Herrero, A., Carpentieri, F., and Calonico, D. Seismic monitoring using the telecom fiber network. *Comm. Earth Env.*, 5, 2024. doi: 10.1038/s43247-024-01338-2.

Dou, S., Lindsey, N., Wagner, A. M., Daley, T. M., Freifeld, B., Robertson, M., Peterson, J., Ulrich, C., Martin, E., and Ajo-Franklin, J. B. Distributed Acoustic Sensing for seismic monitoring of the near surface: A traffic-noise interferometry study. *Sci. Rep.*, 7, 2017. doi: 10.1038/s41598-017-11986-4.

Fang, G., Li, Y. E., Zhao, Y., and Martin, E. R. Urban near-surface seismic monitoring using distributed acoustic sensing. *Geophys. Res. Lett.*, 47, 2020. doi: 10.1029/2019GL086115.

Fichtner, A., Bogris, A., Nikas, T., Bowden, D., Lentas, K., Melis, N. S., Simos, C., Simos, I., and Smolinski, K. Theory of phase transmission fibre-optic sensing. *Geophys. J. Int.*, 231, 2022. doi: 10.1093/gji/ggac237.

Fichtner, A., Hofstede, C., Gebraad, L., Zunino, A., Zigone, D., and Eisen, O. Borehole fibre-optic seismology inside the Northeast Greenland Ice Stream. *Geophys. J. Int.*, 235:2430–2441, 2023a. doi: 10.1093/gji/ggad344.

Fichtner, A., Hofstede, C., Kennett, B. L. N., Nymand, N. F., Lauritzen, M. L., Zigone, D., and Eisen, O. Fiber-optic airplane seismology on the Northeast Greenland Ice Stream. *The Seismic Record*, pages 125–133, 2023b. doi: 10.1785/0320230004.

Hanka, W. and Kind, R. The GEOFON program. *Ann. Geophys.*, 37, 1994. doi: 10.4401/ag-4196.

Hartog, A. *An introduction to distributed optical fibre sensors*. CRC Press, Boca Raton, 2017. doi: 10.1201/9781315119014.

Hudson, T. S., Baird, A. F., Kendall, J. M., Kufner, S. K., Brisbourne, A. M., Smith, A. M., Butcher, A., Chalari, A., and Clarke, A. Distributed Acoustic Sensing (DAS) for natural microseismicity studies: A case study from Antarctica. *J. Geophys. Res.*, 126, 2021. doi: 10.1029/2020JB021493.

Husmann, D., Bernier, L.-G., Bertrand, M., Calonico, D., Chaloulos, K., Clausen, G., Clivati, C., Faist, J., Heiri, E., Hollenstein, U., Johnson, A., Mauchle, F., Meir, Z., Merkt, F., Mura, A., Scalari, G., Scheidegger, S., Schmutz, H., Sinhal, M., Willitsch, S., and Morel, J. SI-traceable frequency dissemination at 1572.06 nm in a stabilized fiber network with ring topology. *Optics Express*, 29:24592–24605, 2021. doi: 10.1364/OE.427921.

Igel, J., Klaasen, S., Noe, S., Nomikou, P., Karantzalos, K., and Fichtner, A. Challenges in submarine fiber-optic earthquake monitoring. *ESS Open Archive*, May 2024, 2024. doi: 10.22541/essoar.171691177.74747140/v1.

Jousset, P., Reinsch, T., Ryberg, T., Blanck, H., Clarke, A., Aghayev, R., Hersir, G. P., Henninges, J., Weber, M., and Krawczyk, C. M. Dynamic strain determination using fibre-optic cables allows imaging of seismological and structural features. *Nat. Comm.*, 9, 2018. doi: 10.1038/s41467-018-04860-y.

Jousset, P., Currenti, G., Schwarz, B., Chalari, A., Tilmann, F., Reinsch, T., Zuccarello, L., Privitera, E., and Krwaczyk, C. M. Fibre optic distributed acoustic sensing of volcanic events. *Nat. Comm.*, 13, 2022. doi: 10.1038/s41467-022-29184-w.

Kikuchi, M. and Kanamori, H. Inversion of complex body waves - III. *Bull. Seis. Soc. Am.*, 81:2335–2350, 1991. doi: DOI:10.1785/bssa0810062335.

Klaasen, S., Paitz, P., Lindner, N., Dettmer, J., and Fichtner, A. Distributed Acoustic Sensing in volcano-glacial environments — Mount Meager, British Columbia. *J. Geophys. Res.*, 159, 2021. doi: 10.1029/2021JB022358.

Klaasen, S., Thrastarson, S., Cubuk-Sabuncu, Y., Jonsdottir, K., Gebraad, L., Paitz, P., and Fichtner, A. Subglacial volcano monitoring with fiber-optic sensing: Grímsvötn, Iceland. *Volcanica*, 6, 2023. doi: 10.30909/vol.06.02.301311.

Lindsey, N. J., Rademacher, H., and Ajo-Franklin, J. B. On the broadband instrument response of fiber-optic DAS arrays. *J. Geophys. Res.*, 125, 2020. doi: org:10.1029/2019JB018145.

Lior, I., Sladen, A., Rivet, D., Ampuero, J.-P., Hello, Y., Becerill, C., Martins, H. F., Lamare, P., Jestin, C., Tsagkli, S., and Markou, C. On the detection capabilities of underwater Distributed Acoustic Sensing. *J. Geophys. Res.*, 2021. doi: 10.1029/2020JB020925.

Marra, G., Clivati, C., Luckett, R., Tampellini, A., Kronjäger, J., Wright, L., Mura, A., Levi, F., Robinson, S., Xuereb, A., Baptie, B., and Calonico, D. Ultrastable laser interferometry for earthquake detection with terrestrial and submarine cables. *Science*, 361: 486–490, 2018. doi: 10.1126/science.aat4458.

Mecozzi, A., Cantono, M., Castellanos, J. C., Kamalov, V., Muller, R., and Zhan, Z. Polarization sensing using submarine optical cables. *Optica*, 8, 2021. doi: 10.1364/OPTICA.424307.

Noe, S., Husmann, D., Müller, N., Morel, J., and Fichtner, A. Long-

range fiber-optic earthquake sensing by active phase noise cancellation. *Sci. Rep.*, 13, 2023. doi: 10.1038/s41598-023-41161-x.

Paitz, P., Edme, P., Gräff, D., Walter, F., Doetsch, J., Chalari, A., Schmelzbach, C., and Fichtner, A. Empirical investigations of the instrument response for distributed acoustic sensing (DAS) across 17 octaves. *Bull. Seis. Soc. Am.*, 111:1–10, 2021. doi: 10.1785/0120200185.

Schioppo, M., Kronjäger, J., Silva, A., Ilieva, R., Paterson, J. W., Baynham, C. F. A., Bowden, W., Hill, I. R., Hobson, R., Vianello, A., Dovale-Álvarez, M., Williams, R. A., Marra, G., Margolis, H. S., Amy-Klein, A., Lopez, O., Cantin, E., Álvarez-Martínez, H., Le Targat, R., Pottie, P. E., Quintin, N., Legero, T., Häfner, S., Sterr, U., Schwarz, R., Dörscher, S., Lisdat, C., Koke, S., Kuhl, A., Waterholter, T., Benkler, E., and Grosche, G. Comparing ultrastable lasers at 7 × 10-17 fractional frequency instability through a 2220 km optical fibre network. *Nature Communications*, 13, 2022. doi: 10.1038/s41467-021-27884-3.

SED. Swiss Seismological Service, earthquake catalog. http://www.seismo.ethz.ch/en/earthquakes/switzerland/all-earthquakes/, 2024. Accessed: 2024-06-21.

Sladen, A., Rivet, D., Ampuero, J. P., de Barros, L., Hello, Y., Calbris, G., and Lamare, P. Distributed sensing of earthquakes and ocean-solid Earth interactions on seafloor telecom cables. *Nat. Comm.*, 10, 2019. doi: 10.1038/s41467-019-13793-z.

Spica, Z. J., Nishida, K., Akuhara, T., Petrelis, F., Shinohara, M., and Yamada, T. Marine sediment characterized by ocean-bottom fiber-optic seismology. *Geophys. Res. Lett.*, 47, 2020a. doi: 10.1029/2020GL088360.

Spica, Z. J., Perton, M., Martin, E. R., Beroza, B. C., and Biondi, B. Urban seismic site characterization by fiber-optic seismology. *J. Geophys. Res.*, 125, 2020b. doi: 10.1029/2019JB018656.

Tarantola, A. and Valette, B. Generalized Nonlinear Inverse Problems Solved Using the Least Squares Criterion. *Rev. Geophys.*, 20:219–232, 1982. doi: 10.1029/RG020i002p00219.

Walter, F., Gräff, D., Lindner, F., Paitz, P., Köpfli, M., Chmiel, M., and Fichtner, A. Distributed Acoustic Sensing of microseismic sources and wave propagation in glaciated terrain. *Nat. Comm.*, 11, 2020. doi: 10.1038/s41467-020-15824.

Zhan, Z., Cantono, M., Kamalov, V., Mecozzi, A., Müller, R., Yin, S., and Castellanos, J. C. Optical polarization-based seismic and water wave sensing on transoceanic cables. *Science*, 371: 931–936, 2021. doi: 10.1126/science.abe6648.